Modeling of the key characteristics of high-efficiency silicon solar cells with planar surfaces

1st Anatoliy Sachenko[a] sach@isp.kiev.ua

2nd Vitaliy Kostylyov[a] vkost@isp.kiev.ua

3rd Viktor Vlasiuk[a] viktorvlasiuk@gmail.com

4th Igor Sokolovskyi[a] i.o.sokolovskyi@gmail.com

5th Mykhaylo Evstigneev[b] mevstigneev@mun.ca

[a]*V. Lashkaryov Institute of Semiconductor Physics, National Academy of Sciences of Ukraine, Kyiv, Ukraine*

[b]*Department of Physics and Physical Oceanography, Memorial University of Newfoundland, St. John's, NL, A1B 3X7, Canada*

2021 IEEE 48th Photovoltaic Specialists Conference (PVSC) | 978-1-6654-1922-2/21/$31.00 ©2021 IEEE | DOI: 10.1109/PVSC43889.2021.9518502

***Abstract*—Short-circuit current, open-circuit voltage, and photoconversion efficiency of silicon back contact solar cells (BCSC) with planar surfaces are calculated theoretically. In addition to the recombination channels usually considered in this kind of modeling, namely, radiative, Auger, Shockley-Read-Hall, and surface recombination, the model also takes into account the nonradiative trap-assisted exciton Auger recombination and recombination in the space-charge region. It is established that these two recombination mechanisms are essential in the BCSCs in the maximum power operation regime. The model results are in good agreement with the experimental results from the literature.**

***Index Terms*—silicon, solar cell, efficiency, space-charge region recombination**

I. Introduction

The vast majority of silicon solar cells (SCs) currently used have one or two textured surfaces [1]. This radically reduces the reflection of light at the air-semiconductor interface. At the same time, there are non-textured silicon-based SCs, in which the reduction of light reflection is achieved by applying antireflection coatings. A special niche is now occupied by silicon SCs with back contact (BCSC). Although they are also mostly textured, but the physical basis of their operation is somewhat different from those of the traditional SC design [2]. In particular, these SCs must have long lifetimes of nonequilibrium charge carriers ($\sim 1\,$ms), which brings them closer to traditional highly efficient textured silicon SCs with two-sided contacts. Second, the rate of surface recombination on the illuminated surface in these SCs should be low enough, which also brings them closer to highly efficient textured silicon SCs. A separate issue for these SCs is to describe the intrinsic quantum efficiency of the photocurrent in the long-wavelength absorption region.

In this work, a theoretical modeling of the key characteristics of the BCSCs is performed. The model takes into account all known components of the effective lifetime in silicon and the peculiarities of the internal quantum efficiency of photocurrent in the long-wavelength absorption region. The obtained theoretical curves are compared to the experimental work [3], and a good agreement between the theory and the experiment is achieved.

II. Effective recombination time in silicon

The general expression for the effective recombination lifetime in Si with the n-type base is

$$\tau_{eff}(n) = \left(\tau_{SRH}^{-1} + \tau_{exc-A}^{-1} + \frac{S_{S0}}{d}\left(1+\frac{\Delta n}{n_0}\right) + \tau_r^{-1}(n) + \tau_A^{-1}(n) + \frac{S_{SC}(n)}{d}\right)^{-1}, \quad (1)$$

where $n = n_0 + \Delta n$ is the total electon concentration, consisting of the equilibrium, n_0, and excess, Δn, contributions; τ_{SRH} is Shockley-Read-Hall (SRH) lifetime; S_{S0} is the net recombination velocity on the front and rear surfaces at low injection level; $\tau_{exc-A}(n) = \tau_{SRH} n_x/n_0$ is the exciton Auger recombination time with $n_x = 8.2\cdot 10^{15}\,\mathrm{cm}^{-3}$ [4]; τ_r is radiative recombination time, τ_A is band-to-band Auger recombination time [5], and d is the base thickness of the SC. In the following, we will assume that τ_{SRH} = const.

It is worthwhile to dwell on the question why most today's simulations do not take into account the non-radiative exciton recombination. This may have to do with the fact that it is masked by the SRH and surface recombination Indeed, redefinition of the SRH time as $\tau^*_{SRH} = \tau_{SRH}/(1 + n_0/n_x)$ and surface recombination velocity as $S^* = S_0 + (S_0 + dn_0/(\tau_{SRH} n_x))\Delta n/n_0$ renders introduction of the non-radiative exciton Auger recombination unnecessary. Note that for $n_0 = 4.9\cdot 10^{15}\,\mathrm{cm}^{-3}$, the value of τ^*_{SRH} is smaller than τ_{SRH} by about 60 %. It should also be noted that an expression for the effective lifetime in Si similar to the formula for τ^*_{SRH} was used in some previous work [6] with $n_x = 7.1\cdot 10^{15}\,\mathrm{cm}^{-3}$.

The inverse radiative lifetime is $1/\tau_r(n) = A(n_0 + \Delta n)$ with the radiative recombination parameter

$$A = \int_0^\infty dE_{ph}\,\alpha(E_{ph})\left(\frac{n_r(E_{ph})E_{ph}}{\pi c\hbar^{3/2} n_i(T)}\right)^2 e^{-E_{ph}/kT}, \quad (2)$$

where the absorption coefficient α and refractive index n_r depend on the photon energy E_{ph} as tabulated in [7]. In order to approximately take into account the bandgap narrowing effect by the amount ΔE_g [8], the argument of the absorption coefficient was shifted by the size of bandgap narrowing energy [9], i.e. $\alpha(E_{ph}) = \alpha_0(E_{ph} + \Delta E_g)$, where α_0 is the absorption coefficient from [7] at zero bandgap narrowing size.

The lifetime due to the recombination in SCR is defined as

$$\tau_{SCR} = d/S_{SCR} \ , \tag{3}$$

where the SCR recombination velocity

$$S_{SCR} = \int_0^\infty dx \, \frac{n_0 + \Delta n}{\tau_{SCR}(x)} \Big((n_0 + \Delta n) e^{y(x)} + n_i e^{E_t/kT} + b_r \left((p_0 + \Delta n) e^{-y(x)} + n_i e^{-E_t/kT} \right) \Big)^{-1} \ . \tag{4}$$

Here, the SCR recombination time $\tau_{SCR}(x)$ is related to the concentration of traps, $N_t(x)$, as $\tau_{SCR}(x) = (V_p \sigma_p N_t(x))^{-1}$, the ratio of the hole-to-electron capture rate constants $b_r = V_p \sigma_p / (V_n \sigma_n)$ is expressed in terms of the electron and hole thermal velocities $V_{n,p}$ and capture cross-sections $\sigma_{n,p}$. The trap energy E_t is measured from the middle of the bandgap, p_0 is the equilibrium hole concentration, n_i is the intrinsic charge carriers concentration, and $y(x)$ is the electric potential normalized to the thermal voltage kT/q. A good agreement between the experiment and the theory can be obtained by assuming that the distribution of the inverse lifetime in the SCR is described by a Gaussian

$$\tau_{SCR}^{-1}(x) = \tau_m^{-1} e^{-(x - x_m)^2/(2\sigma^2)} \ , \tag{5}$$

where τ_m is the lifetime at the maximum point, x_m, and σ is the dispersion. The upper integration limit w in (4) is taken to be $w = x_m + 5\sigma$. A fast decline of $S_{SCR}(\Delta n)$ can be achieved by reducing the width σ of the Gaussian, and large values of S_{SC} at small Δn can be achieved by reducing the maximal lifetime τ_m.

To find the dependence of the non-dimensional potential $y(x)$ on the coordinate x, it is necessary to use the solution of the Poisson equation

$$x = \frac{\lambda_D}{\sqrt{2}} \int_{y_0}^{y} \frac{dy'}{\left(1 + \frac{\Delta n}{n_0}\right)(e^{y'} - 1) - y' + \frac{\Delta n}{n_0}(e^{-y'} - 1)} \tag{6}$$

where $\lambda_D = \sqrt{\frac{\epsilon_0 \epsilon_{Si} kT}{q^2 n_0}}$ is Debye screening length, q is the elementary charge, ϵ_0 the vacuum permittivity, and ϵ_{Si} the dielectric constant of Si. Note that in (4)-(6), the distance x is measured from the rear surface toward the front surface. The initial value of the potential, $y_0 = y(x = 0)$, is found by modeling the n-p$^+$ junction on the p$^+$-side as a thin negatively charged slab with the surface charge density $-qN$, N being the surface concentration of acceptor ions in that slab. Then, from the Poissons equation, y_0 is found from the transcendental equation

$$qN = \sqrt{2kT\epsilon_0\epsilon_{Si}} \sqrt{(n_0 + \Delta n)(e^{y_0} - 1) - n_0 y_0 + \Delta n (e^{-y_0} - 1)} \ . \tag{7}$$

The value of S_{SCR} strongly decreases with the excess concentration of electron-hole pairs Δn and the SRH lifetime in the SCR, τ_m. In indirect-bandgap semiconductors with a small SRH lifetime, the value of S_{SCR} is quite large. Then, SCR recombination competes with the recombination in the neutral bulk at those values of Δn that are realized in the maximum-power operation regime. Therefore, when modeling the SC characteristics, recombination in the SCR should be considered.

Another situation is realized in the high-performance silicon SCs, in particular, in the BCSCs. Their bulk SRH lifetime is of the order of or greater than 1 ms. If we assume that $\tau_m \approx \tau_{SRH}$, then at the voltages typical for the maximum-power operation regime, the value of $S_{SCR} < 10^{-2}$ cm/s and, at a first glance, SCR recombination can be neglected in comparison with other recombination components. But, as the analysis performed in [10], [11] showed, the main difference between recombination in SCR and recombination in the neutral bulk in the case of silicon is that the lifetime in SCR τ_m can be several orders of magnitude smaller than the Shockley-Read-Hall lifetime τ_{SRH}. For the cases analyzed in [10], [11], its value is of the order of 1 μs. This primarily indicates that the concentration of deep levels in the SCR responsible for SRH recombination significantly exceeds the concentration of deep levels in the neutral bulk. The reasons for the increase in the concentration of deep traps in the SCR may have to do with the gettering during the high-temperature diffusion stage to create a p-n junction, the presence of boron complexes that increase the concentration of deep levels, the effects related to the hight electric field strength in the SCR, and other factors. Then, with the ideality factor close to 2, the dark current may be formed by the SCR recombination at voltages up to the maximal-power voltage $V_m \approx 0.55 - 0.65$ V. As a result, the recombination rate of the SCR of highly efficient silicon SCs in the maximum power operation regime becomes comparable to other recombination components, which necessitates taking the SCR recombination into account as well.

III. Photoconversion parameters of the BCSCs

If the minority carriers' diffusion length $L_d = \sqrt{D_p \tau_{eff}}$ is much bigger than one-quarter of the base thickness, d/4, and if the combined surface and SCR recombination velocity $S_{SC} + S_{S0} \ll 2D_p/d$, then the excess concentration profile is practically uniform in the base region. In that case, one can employ the narrow-base approximation and express the illuminated $I - V$ relation as

$$I(V) = I_L - \frac{qA_{SC} d \Delta n}{\tau_{eff}} - \frac{V + IR_S}{R_{SH}} \ , \tag{8}$$

where the first term is the light-generated current, the second term is the recombination current, A_{SC} is the SC area, and R_S and R_{SH} are the series and shunt resistance. The dark current $I_D(V) = -I(V)|_{I_L = 0}$ is

$$I_D(V) = \frac{qA_{SC} d \Delta n}{\tau_{eff}} + \frac{V - I_D R_S}{R_{SH}} \ . \tag{9}$$

The excess carrier concentration is related to the applied voltage by a modified mass action law,

$$(n_0+\Delta n)(p_0+\Delta n)=n_i^2\, e^{(\Delta E_g+q(V-IR_S))/kT}\ , \quad (10)$$

where n_i is the intrinsic concentration at low injection [12] and $\Delta E_g(n_0,\Delta n)$ is the magnitude of the bandgap narrowing in Si [8]. Eq. (10) can be solved for the excess concentration

$$\Delta n=-\frac{n_0}{2}+\sqrt{\frac{n_0^2}{4}+n_i^2 e^{\Delta E_g/kT}(e^{q(V-IR_S)/kT}-1)}\ . \quad (11)$$

Eqs. (8)-(11) need to be solved numerically. The photoconversion efficiency η, as well as the voltage, V_m, current, I_m, and output power, P_m, in the maximum-power operation regime are found by setting the derivative of $P=IV$ with respect to voltage to zero. The open-circuit voltage and the short-circuit current are obtained by setting in (8) I and V to zero, respectively. The value of the excess concentration in the open-circuit mode can be found from the balance equation

$$I_L=\frac{qA_{SC}d\Delta n_{OC}}{\tau_{eff}}+\frac{V_{OC}}{R_{SH}}\ . \quad (12)$$

IV. Spectral dependence of the photocurrent in BCSC

The photocurrent can be found by integrating the product of the incident photon flux with the spectral density $I(\lambda)$ by the external quantum efficiency $EQE(\lambda)$ as

$$J_L=q\int d\lambda\, I(\lambda)\, EQE(\lambda)\ . \quad (13)$$

The external quantum efficiency $EQE(\lambda)$ is related to the internal quantum efficiency $IQE(\lambda)$ and reflection coefficient $R(\lambda)$ by

$$EQE(\lambda)=f\cdot IQE(\lambda)(1-R(\lambda))\ , \quad (14)$$

where the number $f\lesssim 1$ accounts for the partial absorption of the incident radiation by a coating layer outside of the semiconductor. The simple limit approximation for IQE in a SC with specular flat surfaces when the reflection coefficient of the rear surface equals to 1 is

$$IQE(\lambda)=1-e^{-2\alpha(\lambda)d} \quad (15)$$

A more accurate expression can be obtained by solving the stationary diffusion equation

$$D_p\frac{d^2\Delta n(x)}{dx^2}-\frac{\Delta n}{\tau}+\alpha I_0\left(e^{-\alpha x}+R_d e^{\alpha(x-2d)}\right)=0 \quad (16)$$

for the excess carrier concentration Δn, where R_d is the reflection coefficient of the rear surface. The diffusion equation is supplemented by the boundary conditions

$$j(x=0)=-S_0\Delta n(x=0)\ ,\quad \Delta n(x=d)=0\ , \quad (17)$$

where S_0 is the net recombination velocity on the front surface. The solution of this equation is

$$\Delta n(x)=C_1e^{-x/L}+C_2e^{x/L}+\frac{\alpha I_0\tau}{1-(\alpha L)^2}\left(e^{-\alpha x}+R_de^{\alpha(x-2d)}\right) \quad (18)$$

where $L=\sqrt{D_p\tau}$ is the diffusion length of the minority carriers, and the integration constants $C_{1,2}$ are to be found from (17). The internal quantum efficiency $IQE(\lambda)=j(x=d)/I_0$ then becomes

$$IQE(\lambda)=\frac{\alpha L}{1-\alpha^2L^2}\left(\frac{P}{\cosh\frac{d}{L}+\frac{S_0L}{D_p}\sinh\frac{d}{L}}+Q\right)\ ,$$
$$P=\left(\frac{S_0L}{D_p}+\alpha L\right)(1-R_de^{-2\alpha d})+(1+R_d)e^{-d(\alpha+1/L)}\left(1-\frac{S_0L}{D_p}\right)\ ,$$
$$Q=1+R_d+\alpha L(1-R_d)e^{-\alpha d}\ . \quad (19)$$

Shown in Fig. 1 is the spectral dependence if IQE according to (15) (upper curve) and (19) for the special case $R_d=1$. As seen in this figure, when $L=1\,$cm and $S_0=0$, Eqs. (15) and (19) yield identical results. Upon decreasing L, the maximal IQE-values get smaller. Likewise, increasing S_0 also results in the smaller IQE maxima.

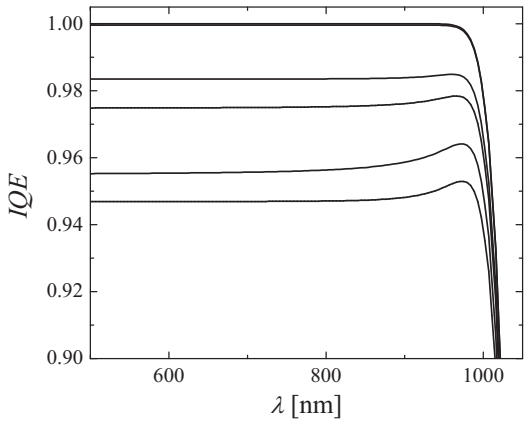

Fig. 1. Theoretical spectral dependence of internal quantum efficiency of BCSC for $d=300\,\mu$m, $R_d=1$. Upper curve: Eq. (15). The remaining curves (from top to bottom) are built for the following values of L (in μm) and S_0 (in cm/s): 10^4 and 0; 1640 and 0; 1640 and 3; 1640 and 10; 900 and 0.

Fig. 2 shows the experimental $EQE(\lambda)$ and $R(\lambda)$ curves for BCSC from [3], as well as the theoretical approximation (19) for $d=300\,\mu$m, $L=0.17\,$cm, and $S_0=3\,$cm/s. As seen in the figure, the theoretical $EQE(\lambda)$ curve agrees with the experimental one very well. Once $EQE(\lambda)$ is known, the dependence of the light-generated photocurrent on the base thickness d follows immediately from (13), allowing us to optimize the SC with respect to this parameter.

V. Results and discussion

We first analyze the results obtained in [3] for a BCSC with the photoconversion efficiency of 19.2 %. To model its key parameters, it is necessary to determine the recombination parameters τ_R and b_r from the measurements of dark $I-V$ curves. In addition, it is necessary to find the SRH lifetime and

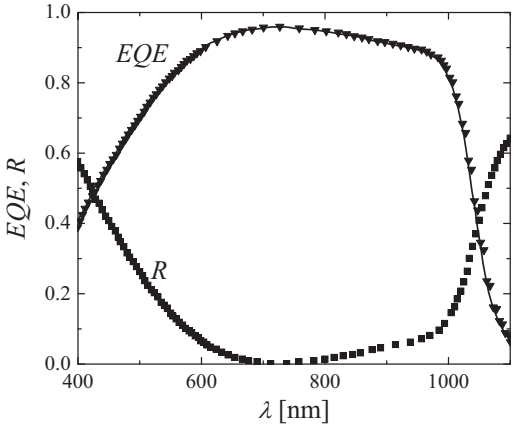

Fig. 2. Experimental (symbols) and theoretical (line) spectral dependence of EQE and the reflection coefficient R of BCSC.

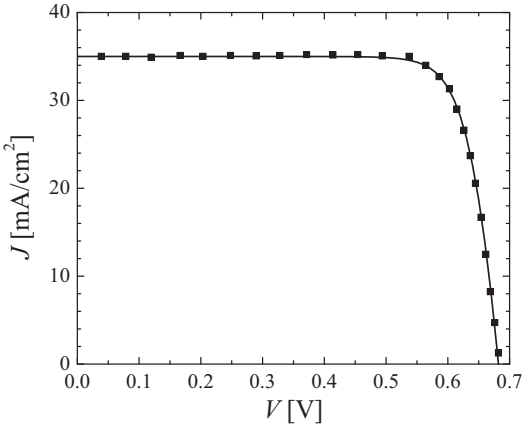

Fig. 4. Experimental (symbols) and theoretical (solid line) illuminated $I-V$ curve of BCSC from [3].

surface recombination velocity. Fig. 3 shows the experimental dependences of the dark current density for the SCs studied on the applied voltage at a temperature of 25 °C, while Fig. 4 shows the experimental dependences for the light generated current density as a function of the applied voltage under the AM1.5 conditions. The dependence $S_{SCR}(\Delta n)$ at these parameters is showin in the insert in Fig. 3.

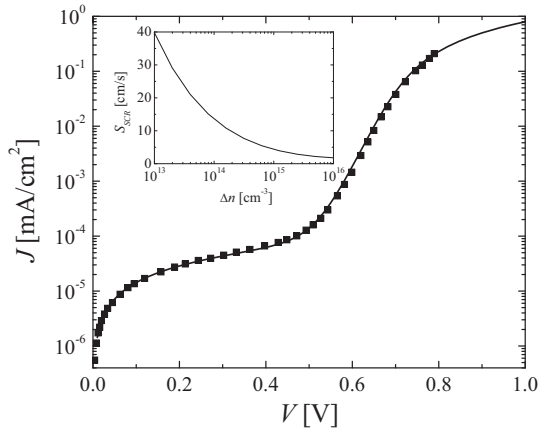

Fig. 3. Experimental (symbols) and theoretical (solid line) dark $I-V$ curves. The insert shows a theoretical $S_{SCR}(\Delta n)$ curve.

Fig. 5 shows the experimental and theoretical effective and bulk lifetimes for the freshly formed SCs (before metallization) vs. the excess concentration of charge carriers. A good fit is achieved by using the following parameters: $\tau_m = 3.8\,\mu$s, $x_m = 85\,$nm, $\sigma = 24\,$nm, $b_r = 0.1$, $\tau_{SRH} = 2.1\,$ms, $S_{0S} = 17.4\,$cm/s, $R_S = 0.64\,\Omega{\cdot}$cm^2. With these parameters, one can also build the theoretical curve of effective lifetime as a function of Δn, shown in Fig. 5. As can be seen from this figure, in the region $\Delta n < 10^{15}\,$cm^{-3}, the effective lifetime increases with Δn. This has to do with the recombination in the SCR. Incidentally, the point of maximum power in this case happens to be $1.96 \cdot 10^{14}\,$cm^{-3}, and the effective lifetime at this point is 0.56 ms. When $\Delta n = 1.96 \cdot 10^{14}\,$cm^{-3}, the SCR and surface recombination velocities are 9.7 cm/s and 18.1 cm/s, respectively, i.e. they are commensurate with each other.

The obvious discrepancies between the experimental and the theoretical curves in Fig. 5 can be explained by the fact that the experimental dependences of $\tau_b(\Delta n)$ is given not for the case of SC, but for the material from which this SC is made. To obtain the correct curve for the SC, one needs to use the dependence of illuminance versus the open-circuit voltage, shown in Fig. 6. This can be done with the help of Eq. (12). The dependence of $\tau_{eff}(\Delta n)$ obtained using the above parameters is shown in Fig. 5. The same figure shows the dependence of $\tau_b(\Delta n)$ calculated using expressions for different components of recombination time. As can be seen from the figure, the values of and τ_{eff} and τ_b differ for the cases of the SC material and SC itself. From the constructed $\tau_{eff}(\Delta n)$ curve it is seen that in the region $\Delta n < 10^{15}\,$cm^{-3} an increasing section is realized due to recombination in SCR.

With the above parameters, the open-circuit voltage calculated using the experimental value of the short-circuit current density of 35 mA/cm^2, is 682 mV, which is completely identical to the experimental value. The calculation of the photoconversion efficiency with the above parameters and the value of the series resistance of $0.64\,\Omega{\cdot}$cm^2, gives a value of 19.2 %, which also coincides with the experimental value. With the theoretical values of V_m and J_m, the fill factor equals 0.805, which coincides with the experimental value [3]. In the same way, the key parameters of the other three SCs can be calculated. A comparison of the experimental (see Table 1 of [3]) and the theoretical parameter values is given in Table I.

In addition to the key SC parameters, Table I shows the value of S_{S0} and of the series resistance calculated in two approximations. In the first approximation, the R_S was obtained

TABLE I
PARAMETERS OBTAINED BY FITTING THE EXPERIMENTAL RESULTS FROM [3]

No.	V_{OC}, V	FF, %	η, %	S_{S0}, cm/s	R_{Sexp}, Ω·cm^2	R_{Sthry} Ω·cm^2	R_{S1thry}, Ω·cm^2
1	683.2	78.2	18.7	15.7	1.3	1.09	1.03
2	681.4	80.4	19.1	18.2	0.9	0.67	0.65
3	682.5	79.4	18.9	16.6	1.1	0.74	0.71
4	682.0	80.5	19.2	17.4	0.8	0.64	0.63

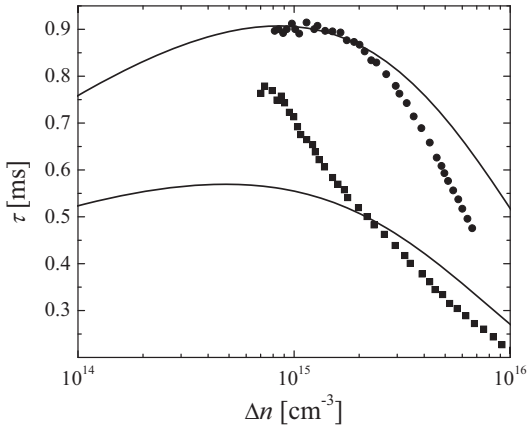

Fig. 5. Experimental (symbols) and theoretical (solid lines) bulk (upper curve) and effective (lower curve) lifetimes vs. excess concentration for the BCSC from [3].

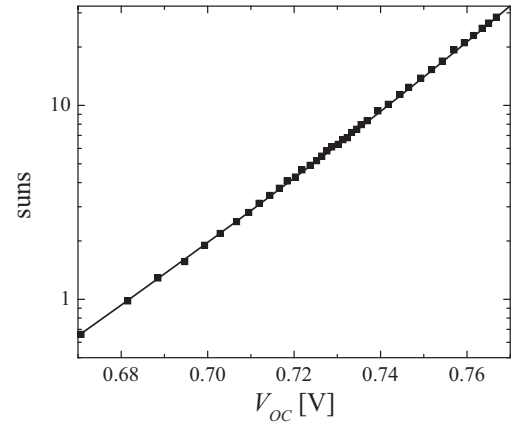

Fig. 6. Experimental (points) and theoretical (line) dependences of illuminance versus open-circuit voltage.

from fitting the experimental and theoretical photoconversion efficiency curves (see the penultimate column in Table I). In the second approach (the last column in Table I), the values of the series resistance were calculated as

$$R_{S1} = \left(1 - \frac{\eta}{\eta(R_S = 0)}\right) \frac{V_m}{J_m} = \left(1 - \frac{FF}{FF(R_S = 0)}\right) \frac{V_m}{J_m} . \quad (20)$$

The theoretical values of the key parameters in Table I agree with the experimental ones with accuracy of better than 0.1 %, which significantly exceeds the experimental error. With respect to the experimental and calculated series resistance values, the differences are much larger. The smallest discrepancy between the two theoretical methods above is about 3 %. The biggest difference between the theoretical and experimental R_S-values from Table I is about 40 %.

In [3], the method of measuring the series resistance is not explained. Usually, the method of two intensities is used for this purpose. This method does not take into account the corrections associated with the bandgap narrowing, which should lead to an increase in the series resistance value. Note also that expression (20) is approximate, whereas the most accurate value of R_S is found by fitting the experimental photoconversion efficiency results.

Table I also shows the low-signal values of surface recombination velocity S_{S0} in different SCs. As can be seen from the table, there is a clear correlation between the open-circuit voltage and the values of S_{S0}: namely, the smaller the former the higher the latter.

Shown in Fig. 7, solid line, is the theoretical photoconversion efficiency vs. the base doping level curve for the SCs with an efficiency of 19.2 % from [3]. As can be seen from the figure, the maximum the photoconversion efficiency of 19.3 % is realized at the level of base doping of $1.2 \cdot 10^{16}$ cm^{-3}. The efficiency value at $n_0 = 4.9 \cdot 10^{15}$ cm^{-3} used in [3] is smaller than the maximum efficiency by 0.1 %.

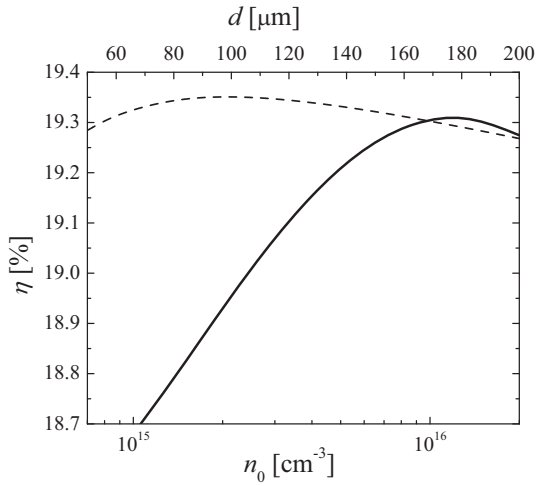

Fig. 7. Theoretical photoconversion efficiency vs. doping level (solid) and base thickness (dash).

Fig. 7 shows also the theoretical photoconversion efficiency

of the same BCSC parameters [3] as a function of the base thickness (dashed line). As can be seen from the figure, the maximum efficiency of 19.4 % occurs at the base thickness of 95 μm. The relative difference between the maximal value and the value at the base thickness of 300 μm used in [3] is 1 %.

Thus, this approach allows both to theoretically describe the key parameters of the high-performance silicon SCs with flat surfaces and to obtain optimal values of their thickness and doping level.

VI. Conclusions

The performance of silicon SCs with a flat surface [3] is analyzed within the thin base approximation. It is shown that near the absorption edge, its internal quantum efficiency is described by $1 - e^{-2\alpha(\lambda)d}$ at large minority carriers' diffusion length and small surface recombination velocity; a general expression for the IQE is obtained for arbitrary values of these parameters. The calculations take into account all known recombination mechanisms in silicon, namely, Shockley-Read-Hall recombination, surface recombination, recombination in the SCR, radiative recombination, nonradiative excitonic trap-assisted Auger recombination, and band-to-band Auger recombination. An important parameter is determined: the recombination lifetime in the SCR. It is shown that including the nonradiative exciton recombination into consideration is equivalent to the renormalization of the SRH lifetime. The difference between the true and the effective SRH lifetimes increases with the doping concentration. The proposed approach allows calculating the key photovoltaic parameters: short-circuit current density, open-circuit voltage, and the fill factor and photoconversion efficiency. A comparison of the theoretical results with the experimental curves for the four SC samples from [3] showed almost perfect agreement and allowed calculating optimal values of the doping level and base thickness for those SCs.

Acknowledgment

This work was partially supported (V. Kostylyov, V. Vlasiuk) by the National Research Foundation of Ukraine (project 2020.02/0036: "Development of physical basis of both acoustically controlled modification and machine learning-oriented characterization for silicon solar cells"). M. Evstigneev is grateful to the Natural Sciences and Engineering Research Council of Canada (NSERC) for financial support and to the Atlantic Computational Excellence Network (ACENet) for computational resources.

References

[1] M.A. Green, "Third generation photovoltaics. Advanced solar energy conversion", Springer (2006).

[2] A.V. Sachenko, A.P. Gorban, V.P. Kostylyov, A.A. Serba, I.O. Sokolovskyi, "Comparative analysis of photoconversion efficiency in the Si solar cells under concentrated illumination for the standard and rear geometries of arrangement of contacts", *Semiconductors*, vol. 41(10), pp. 1214-1223, 2007.

[3] N. Zin, A. Blakers, K. McIntosh, E. Franklin, T. Kho, J. Wong, T. Mueller, A.G. Aberle, Z. Feng, and Q. Huang, "19 % efficient n-type all-back-contact silicon wafer solar cells with planar front surface", *Proceedings of the 49th Australian Solar Energy Society's (AuSES) Conference*, Sydney, Australia, 2011.

[4] A.V. Sachenko, V.P. Kostylyov, V.M. Vlasyuk, I.O. Sokolovskyi , and M. Evstigneev, "The influence of the exciton nonradiative recombination in silicon on the photoconversion efficiency", *Proceedings of the 32 European Photovoltaic Solar Energy Conf. and Exhib.*, pp. 141-147, Munich, 2016.

[5] A. Richter, S. Glunz, F. Werner, J. Schmidt, and A. Cuevas, "Improved quantitative description of Auger recombination in crystalline silicon", *Phys. Rev. B*, vol. 86, pp. 165202:1-14 , 2012.

[6] J.G. Fossum, "Computer-aided numerical analysis of silicon solar cells", *Solid State Electron.*, vol. 19 (4), pp. 269-277 (1976).

[7] M.A. Green, "Self-consistent optical parameters of intrinsic silicon at 300 K including temperature coefficients. Sol. Energy Mater. Sol. Cells", *Sol. Energy Mater. Sol. Cells*, vol. 92, pp. 1305-1310 , 2008.

[8] A. Schenk, "Finite-temperature full random-phase approximation mode of band gap narrowing for silicon device simulation", *J. Appl. Phys.*, vol. 84, pp. 3684-3695, 1998.

[9] A. Sachenko, V. Kostylyov, I. Sokolovskyi, and M. Evstigneev, "Effect of Temperature on Limit Photoconversion Efficiency in Silicon Solar Cells", *IEEE J. Photovolt.*, vol. 10, pp. 63-69, 2020. DOI: 10.1109/JPHOTOV.2019.2949418.

[10] A.V. Sachenko, V.P. Kostylyov, V.M. Vlasiuk, R.M. Korkishko, I.O. Sokolovskyi, V.V. Chernenko, "Features in the formation of a recombination current in the space charge region of silicon solar cells", *Ukr. J. Phys.*, vol. 61, pp. 917-922, 2016.

[11] A.V. Sachenko, V.P. Kostylyov, I.O. Sokolovskyi, A.V. Bobyl', V.N. Verbitskii, E.I. Terukov and M.Z. Shvarts, "Specific features of current flow in α-Si:H/Si heterojunction solar cells", *Tech. Phys. Lett.*, vol. 43, pp. 152155, 2017.

[12] T. Trupke, M.A .Green, P. Wurfel, P.P. Altermatt, A. Wang, J. Zhao, and R. Corkish, "Temperature dependence of the radiative recombination coefficient of intrinsic crystalline silicon", *J. Appl. Phys.*, vol. 94, pp. 4930-4937, 2003.